

Extraction of acoustic normal mode depth functions using vertical line array data

Tracianne B. Neilsen and Evan K. Westwood

Applied Research Laboratories, The University of Texas at Austin, P.O. Box 8029, Austin, Texas 78713-8029

(Received 24 January 2001; revised 27 August 2001; accepted 5 November 2001)

A method for extracting the normal modes of acoustic propagation in the shallow ocean from sound recorded on a vertical line array (VLA) of hydrophones as a source travels nearby is presented. The mode extraction is accomplished by performing a singular value decomposition (SVD) of individual frequency components of the signal's temporally averaged, spatial cross-spectral density matrix. The SVD produces a matrix containing a mutually orthogonal set of basis functions, which are proportional to the depth-dependent normal modes, and a diagonal matrix containing the singular values, which are proportional to the modal source excitations and mode eigenvalues. The conditions under which the method is expected to work are found to be (1) sufficient depth sampling of the propagating modes by the VLA receivers; (2) sufficient source-VLA range sampling, and (3) sufficient range interval traversed by the source. The mode extraction method is applied to data from the Area Characterization Test II, conducted in September 1993 in the Hudson Canyon Area off the New Jersey coast. Modes are successfully extracted from cw tones recorded while (1) the source traveled along a range-independent track with constant bathymetry and (2) the source traveled up-slope with gradual changes in bathymetry. In addition, modes are successfully extracted at multiple frequencies from ambient noise. © 2002 Acoustical Society of America.
[DOI: 10.1121/1.1432982]

PACS numbers: 43.30.Bp, 43.30.Xm, 43.30.Wi [DLB]

I. INTRODUCTION

This paper investigates a method for determining the depth-dependent mode functions of underwater acoustic propagation using measurements on a vertical line array (VLA). The approach does not require any *a priori* information about the sound-speed profile in the water column or the geoacoustic profile of the bottom. The focus of this paper is on using a loud source of opportunity, such as a passing ship, to provide the data from which the mode functions are obtained.

Although we refer to the procedure just described as “mode extraction,” that term has also been used for the procedure of matching modeled mode shapes to measured data on a VLA to decompose the field into modal components (see, for example, Ref. 1). This method allows the different modal contributions to be identified and isolated, but it requires an estimate of the ocean's acoustic parameters to generate the modeled mode shapes. In contrast, the objective of the current method is to extract mode shapes from VLA data directly, with no *a priori* information.

The mode extraction technique explored here is similar to several other approaches that use an eigenvalue decomposition of a spatial cross-spectral density matrix \mathbf{C} to obtain the depth-dependent mode functions. In Ref. 2, a dominant source at a fixed range is assumed, \mathbf{C} is formed by averaging the outer products of measured pressure spectra over multiple-frequency bins in a narrow band, and a requirement related to the temporal separation of the modal pulse arrivals is derived. In Refs. 3 and 4, ambient noise from the ocean surface is assumed, and \mathbf{C} is formed by averaging over time.

In the present work, a dominant source traversing a significant range interval is assumed, \mathbf{C} is formed by averaging over time, and a requirement related to the range interval is derived.⁵ This approach was also used in Ref. 6.

The remainder of the paper is organized as follows. In Sec. II the required experimental setup, the theory of singular value decomposition (SVD), and its relationship to the expression for the pressure field as a sum over the depth-dependent normal modes are presented. The requirements for the SVD of the pressure field to yield reliable depth-dependent normal modes are examined, and the efficiency advantages of performing the SVD on the cross-spectral density matrix are then outlined. This is followed by a brief explanation of how the multiple-frequency and ambient-noise approaches are related to the current work.

Section III contains the results of mode extraction performed using experimental data taken in the Hudson Canyon area in September 1993.⁷ Results are shown for mode extraction using data from a towed cw source. First, the results using data recorded along a range-independent source track are presented, followed by the results using data from a slightly range-dependent source track. Finally, the results of mode extraction using ambient noise recorded prior to the experiment are given. In the concluding section, Sec. IV, the mode extraction technique and results are summarized, and applications of the method are discussed.

II. THEORY: MODE EXTRACTION FROM VLA DATA

The experimental setup required for the mode extraction technique consists of a source moving outward in range in

the vicinity of a vertical line array (VLA) of N_Z hydrophones, as shown in Fig. 1(a). The sound pressure at each hydrophone is recorded over a time interval during which the source–receiver range is r_1, r_2, \dots, r_{N_R} , where N_R is the total number of ranges. An equivalent experimental setup in a range-invariant environment consists of a stationary source in the vicinity of a moving VLA, as shown in Fig. 1(b). In both cases, the pressure time series is measured at each of the N_Z receiver depths and at each of the N_R source–receiver ranges. The frequency components of the time series are obtained by performing a fast Fourier transform (FFT). For an FFT integration time T_w , the frequency bin spacing is $\Delta f = 1/T_w$. For each frequency component or bin, the FFT yields an $N_Z \times N_R$ complex matrix \mathbf{P}

$$\mathbf{P} = \begin{bmatrix} p(z_1, r_1) & p(z_1, r_2) & \cdots & p(z_1, r_{N_R}) \\ p(z_2, r_1) & p(z_2, r_2) & \cdots & p(z_2, r_{N_R}) \\ \vdots & \vdots & \ddots & \vdots \\ p(z_{N_Z}, r_1) & p(z_{N_Z}, r_2) & \cdots & p(z_{N_Z}, r_{N_R}) \end{bmatrix}. \quad (1)$$

The elements of \mathbf{P} may be written according to normal-mode theory as

$$p_{ij} \equiv p(z_i, r_j) = \frac{\sqrt{2\pi} e^{i\pi/4}}{\rho(z_s)} \sum_{m=1}^{N_M} \bar{\phi}_n(z_s) \bar{\phi}_n(z_i) \frac{e^{ik_n r_j}}{\sqrt{k_n r_j}}, \quad (2)$$

where $\bar{\phi}_n(z)$ are the orthonormal, depth-dependent mode functions. For the trapped modes, it is a good approximation that

$$\int_0^H \frac{\bar{\phi}_n(z) \bar{\phi}_m(z)}{\rho(z)} dz = \delta_{nm}, \quad (3)$$

where H is the depth of the half-space.⁸ The expression for $p(z_i, r_j)$ is used to demonstrate how a matrix operation called singular value decomposition (SVD) can yield the depth-dependent modes $\bar{\phi}_n(z)$. We first describe the general properties of the SVD and then explain how the SVD of the matrix \mathbf{P} produces the depth-dependent modes.

A. Singular value decomposition

The SVD of an $N \times M$ complex matrix \mathbf{A} is

$$\mathbf{A} = \mathbf{U} \mathbf{S} \mathbf{V}^\dagger, \quad (4)$$

where \dagger indicates the conjugate transpose of the matrix, \mathbf{S} is a real diagonal matrix with elements in order from largest to smallest down the diagonal, and the columns of both \mathbf{U} and \mathbf{V} satisfy the orthonormality condition

$$\sum_{i=1}^N U_{in} U_{im}^* = \sum_{i=1}^M V_{in} V_{im}^* = \delta_{nm}, \quad (5)$$

where $*$ indicates complex conjugation. Since \mathbf{S} is diagonal, each element of \mathbf{A} may be written as

$$a_{ij} = \sum_{k=1}^N u_{ik} s_{kk} v_{kj}^*. \quad (6)$$

B. The connection between the SVD and the normal modes

Recognizing the similarity between the orthonormality conditions of the modes in Eq. (3) and the singular vectors in Eq. (5), we express the pressure matrix \mathbf{P} , defined by its elements in Eq. (2), as a product of matrices as in Eq. (4)

$$\mathbf{P} = e^{i\pi/4} \bar{\Phi} \mathbf{\Lambda} \mathbf{R}, \quad (7)$$

where $\bar{\Phi}$, $\mathbf{\Lambda}$, and \mathbf{R} are given by

$$\bar{\Phi} = \frac{1}{\sqrt{\rho(z_s)}} \begin{bmatrix} \bar{\phi}_1(z_1) & \bar{\phi}_2(z_1) & \cdots & \bar{\phi}_{N_M}(z_1) \\ \bar{\phi}_1(z_2) & \bar{\phi}_2(z_2) & \cdots & \bar{\phi}_{N_M}(z_2) \\ \vdots & \vdots & \ddots & \vdots \\ \bar{\phi}_1(z_{N_Z}) & \bar{\phi}_2(z_{N_Z}) & \cdots & \bar{\phi}_{N_M}(z_{N_Z}) \end{bmatrix}, \quad (8)$$

$$\mathbf{\Lambda} = \frac{\sqrt{2\pi N_R}}{\sqrt{\rho(z_s)}} \begin{bmatrix} \frac{1}{\sqrt{k_1}} \bar{\phi}_1(z_s) & 0 & \cdots & 0 \\ 0 & \frac{1}{\sqrt{k_2}} \bar{\phi}_2(z_s) & \cdots & 0 \\ \vdots & \vdots & \ddots & \vdots \\ 0 & 0 & \cdots & \frac{1}{\sqrt{k_{N_M}}} \bar{\phi}_{N_M}(z_s) \end{bmatrix}, \quad (9)$$

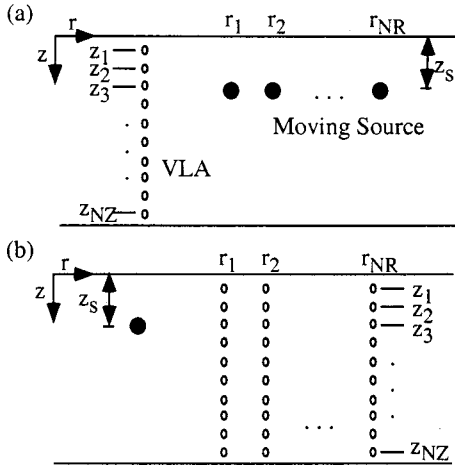


FIG. 1. Plot (a) shows a source (solid dots) moving in the vicinity of a vertical line array (VLA) of hydrophones (circles). The source depth is z_s , and the source to VLA ranges at successive times are r_j , with $j = 1, \dots, N_R$. The hydrophones on the VLA are at depths z_i , with $i = 1, \dots, N_Z$. Plot (b) illustrates an equivalent geometry in a range-invariant environment, namely a stationary source at depth z_s (solid dot) with a moving VLA. The VLA is shown at different times, corresponding to the source–receiver ranges r_j with $j = 1, \dots, N_R$.

$$\mathbf{R} = \frac{1}{\sqrt{N_R}} \begin{bmatrix} \frac{e^{ik_1 r_1}}{\sqrt{r_1}} & \dots & \frac{e^{ik_1 r_{N_R}}}{\sqrt{r_{N_R}}} \\ \frac{e^{ik_2 r_1}}{\sqrt{r_1}} & \dots & \frac{e^{ik_2 r_{N_R}}}{\sqrt{r_{N_R}}} \\ \vdots & \ddots & \vdots \\ \frac{e^{ik_{N_M} r_1}}{\sqrt{r_1}} & \dots & \frac{e^{ik_{N_M} r_{N_R}}}{\sqrt{r_{N_R}}} \end{bmatrix}, \quad (10)$$

where factors of $\sqrt{N_R}$ and $1/\sqrt{N_R}$ have been included in Eqs. (9) and (10), respectively, to reflect the size of the statistical ensemble.

We now examine the conditions under which the mode decomposition matrices $\bar{\Phi}$, Λ , and \mathbf{R} correspond to the singular value decomposition matrices \mathbf{U} , \mathbf{S} , and \mathbf{V} . In order for $\bar{\Phi}$ in Eq. (8) to correspond to \mathbf{U} of Eq. (4), the orthonormality condition given in Eq. (5) must hold:

$$\sum_{i=1}^{N_Z} \bar{\Phi}_{in} \bar{\Phi}_{im}^* = \sum_{i=1}^{N_Z} \frac{\bar{\phi}_n(z_i) \bar{\phi}_m^*(z_i)}{\rho(z_s)} \stackrel{?}{=} \delta_{nm}, \quad (11)$$

where the notation $\stackrel{?}{=}$ indicates an approximate equality that has not yet been demonstrated.

The summation in Eq. (11) is a good approximation to the integral in Eq. (3) provided that (1) the mode functions are well sampled by the receivers in depth; (2) the density of the water is nearly constant; and (3) the possibly nonuniform depth sampling is accounted for by weighting each term of the summation in Eq. (11) by the average element spacing. Clearly, modes that have significant amplitudes in the bottom cannot be well sampled by a VLA in the water column. Therefore, the fields at short ranges, where bottom-penetrating modes are significant, should not be used to form \mathbf{P} in Eq. (1).

The matrix Λ in Eq. (9) corresponds to the matrix \mathbf{S} in Eq. (4) because it is diagonal and predominantly real. The latter condition holds because, especially for the modes that propagate to fairly long ranges, $\text{Re}(k_n) \gg \text{Im}(k_n)$ and $\text{Re}(\bar{\phi}_n) \gg \text{Im}(\bar{\phi}_n)$. Note that the diagonal elements of Λ are not necessarily in decreasing order but may be rearranged to be so as long as the corresponding columns of $\bar{\Phi}$ and the rows of \mathbf{R} are also rearranged. Because the values of Λ are proportional to the modal source excitation, the strongest propagating modes are found in the left-most columns of \mathbf{U} .

An important point regarding the matrix \mathbf{S} is that if two or more of the singular values in \mathbf{S} are nearly equal, the corresponding singular vectors in \mathbf{U} are not uniquely determined,⁹ and, as a result, the desired depth-dependent modes are linear combinations of the columns of \mathbf{U} . A good criterion for determining when extracted mode functions are not valid, developed by examining simulated data, is that those with adjacent singular values within 5%–10% of each other, when scaled by the largest singular value, can be degenerate, although many are well extracted.¹⁰ Problems associated with close adjacent singular values are more likely to occur at higher frequencies because more modes are present in the waveguide, and hence there is a higher probability of two modes having close modal source excitations.

Finally, with regard to the third matrices of Eqs. (7) and (4), \mathbf{R} of Eq. (10) must satisfy Eq. (5)

$$\sum_{j=1}^{N_R} R_{nj} R_{mj}^* = \sum_{j=1}^{N_R} \frac{e^{i(k_n - k_m^*) r_j}}{N_R r_j} \stackrel{?}{=} \delta_{nm}. \quad (12)$$

In order for all the columns of \mathbf{P} to be weighted equally, the following amplitude normalization is performed:

$$\sum_{i=1}^{N_Z} p(z_i, r_j) p(z_i, r_j)^* = 1. \quad (13)$$

As a result, the loss factors and the relative source amplitudes are effectively removed from the field \mathbf{P} . After the amplitude normalization, the orthonormality condition in Eq. (12) becomes

$$D_{nm} = \sum_{j=1}^{N_R} R_{nj} R_{mj}^* = \sum_{j=1}^{N_R} \frac{e^{i \text{Re}(k_n - k_m) r_j}}{N_R} \stackrel{?}{=} \delta_{nm}. \quad (14)$$

The number of revolutions the elements of the sum D_{nm} complete in the complex plane is

$$n_{\text{rot}} = \frac{\text{Re}(k_n - k_m) \Delta r}{2\pi}, \quad (15)$$

where $\Delta r = r_{\text{max}} - r_{\text{min}}$ is the range interval. The dependence of $|D_{nm}|$ on n_{rot} is illustrated in Fig. 2. Details regarding the parameters used are given in the figure caption. It is clear from Fig. 2 that as n_{rot} increases, the exponential terms in the summation, for $n \neq m$, tend to cancel out, and the numerator of Eq. (14) is much less than the denominator N_R . Thus, when n_{rot} is large, the off-diagonal components of $\mathbf{R}\mathbf{R}^\dagger$ are very small, and Eq. (14) holds approximately.

Guidelines have been developed, using simulated data, for selecting approximate source–VLA ranges that make Eq. (14) hold and thus optimize the performance of the mode

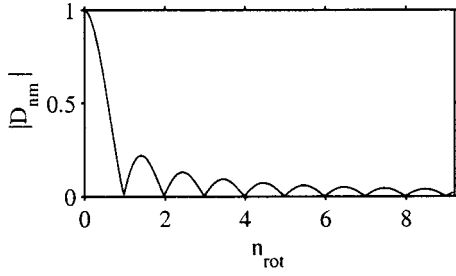


FIG. 2. Dependence of $|D_{nm}|$ from Eq. (14) on n_{rot} from Eq. (15). In constructing the plot, r_{min} was taken to be 6 km and r_{max} was varied from 6–14 km, causing n_{rot} to increase from 0 to 9.2. The value $\text{Re}(k_n - k_m) = 0.0072$ was taken to be the minimum eigenvalue separation for 200-Hz propagation in the ACT-II environment examined in Sec. III.

extraction technique. First, the range sampling dr should be sufficiently small that the field is sampled in range (or time) finely compared to the minimum interference distance, defined by the maximum difference in horizontal wave number

$$(dr) \ll (C_{nm})_{\text{min}}, \quad (16)$$

where $C_{nm} = 2\pi/|k_m - k_n|$ is the modal cycle distance.

Second, the approximate range interval traversed by the source should be large compared to the maximum modal cycle distance

$$\Delta r \gg (C_{nm})_{\text{max}}, \quad (17)$$

which means the elements of the sum in Eq. (14) complete a large number of revolutions in the complex plane. In shallow water, this condition is typically most difficult to achieve for neighboring low-order modes.

Third, the number of significant propagating modes should be relatively constant over the range interval. In shallow water, the trapped modes often have exponentially decaying tails in the bottom and are attenuated as they travel from the source to the receivers. When the number of significant modes changes within the range interval, the form of \mathbf{P} no longer fits that of the SVD, and the mode extraction is less successful. A constant number of propagating modes is a frequency-dependent condition that is more stringent for higher frequencies. Thus, a large range extent Δr and a small range ratio $r_{\text{max}}/r_{\text{min}}$ is the ideal case because the same amount of relative modal attenuation occurs each time the range is doubled.

In summary, the optimum conditions for the SVD of \mathbf{P} to result in a matrix \mathbf{U} that corresponds to the depth-dependent mode functions are (1) the receivers must sample the propagating modes sufficiently well in depth; (2) the range extent Δr must be sufficiently large and sampled finely; and (3) the number of propagating modes over the range interval needs to be fairly constant. An additional requirement is that the signal-to-noise ratio needs to be positive. Since no information about the source, such as depth, exact range, or relative phase is needed, the mode extraction can be performed using a source of opportunity such as a passing ship.

Although the modes can be extracted by performing an SVD on the $N_Z \times N_R$ pressure matrix \mathbf{P} at each frequency, the efficiency of the calculation can be improved, since typically,

$N_Z \ll N_R$, by using the cross-spectral density matrix $\mathbf{C} = \mathbf{P}\mathbf{P}^\dagger$ instead. The cross-spectral density matrix at each frequency is a square $N_Z \times N_Z$ matrix that may be obtained by range averaging the outer products of the depth-dependent fields $\bar{p}(r_n)$

$$\begin{aligned} \mathbf{C} = \mathbf{P}\mathbf{P}^\dagger &= \begin{bmatrix} \bar{p}(r_1) \\ \vdots \\ \bar{p}(r_{N_R}) \end{bmatrix} [\bar{p}(r_1), \dots, \bar{p}(r_{N_R})] \\ &= \sum_{n=1}^{N_R} \bar{p}(r_n) \bar{p}^\dagger(r_n). \end{aligned} \quad (18)$$

Using the matrix representation of \mathbf{P} in Eq. (7), \mathbf{C} can be expressed as a product of three matrices

$$\mathbf{C} = \mathbf{P}\mathbf{P}^\dagger = \bar{\Phi} \Lambda \mathbf{R} \mathbf{R}^\dagger \Lambda^\dagger \bar{\Phi}^\dagger \approx \bar{\Phi} \Lambda^2 \bar{\Phi}^\dagger, \quad (19)$$

where $\mathbf{R}\mathbf{R}^\dagger \approx \mathbf{1}$ when the conditions for orthonormality, discussed previously, are met. Therefore, the three matrices returned from an SVD of \mathbf{C} can be identified as $\mathbf{U} = \mathbf{V} = \bar{\Phi}$ and $\mathbf{S} = \Lambda^2$. Note that \mathbf{C} is Hermitian, and, therefore, an SVD of \mathbf{C} produces identical \mathbf{U} and \mathbf{V} matrices. In addition, the number of VLA receivers N_Z must be at least as large as the number of propagating modes that contribute significantly to the field.

C. Additional configurations for mode extraction

The argument has been presented that a source traversing a sufficiently large range extent produces a pressure matrix \mathbf{P} on a VLA that can be expressed as the product of three matrices that satisfy the same conditions as the matrices obtained from the singular value decomposition. Two other source–receiver configurations have been shown to lead to a pressure matrix that can be similarly decomposed. The requirement for successful mode extraction in each case is that the third matrix in a matrix representation of \mathbf{P} [see Eq. (7)] be approximately orthonormal [$\mathbf{R}\mathbf{R}^\dagger \approx \mathbf{1}$]. When this condition holds, the spatial cross-spectral density matrix \mathbf{C} reduces to the expression in Eq. (19), and the SVD of \mathbf{C} yields the mode functions. Brief derivations of the two other approaches are given below.

1. Single range and multiple frequencies

In Ref. 2, the pressure field in a narrow frequency band B at a single source–VLA range r_o is used to construct an $N_Z \times N_F$ pressure matrix \mathbf{P} versus depth and frequency bin. The elements of \mathbf{P} are expressed, similar to Eq. (2), as

$$p_{ij} \equiv p(z_i, f_j) = \frac{\sqrt{2\pi} e^{i\pi/4}}{\rho(z_s)} \sum_{n=1}^{N_M} \bar{\phi}_n(z_s) \bar{\phi}_n(z_i) \frac{e^{ik_n(f_j)r_o}}{\sqrt{k_n(f_j)r_o}}, \quad (20)$$

where the mode functions $\bar{\phi}_n(z)$, which in reality depend weakly on frequency, are assumed constant over the bandwidth in order to perform the following decomposition. \mathbf{P} can be expressed as the product of three matrices, as in Eq. (7)

$$\mathbf{P} = e^{i\pi/4} \bar{\Phi} \Lambda \mathbf{F}, \quad (21)$$

where $\bar{\Phi}$ is given by Eq. (8), $\Lambda_{\mathbf{F}}$ is a real, diagonal matrix, and the elements of \mathbf{F} are

$$F_{nj} = \frac{e^{ik_n(f_j)r_o}}{\sqrt{N_F k_n(f_j)}}. \quad (22)$$

The orthonormality condition, $\mathbf{F}\mathbf{F}^\dagger \approx \mathbf{1}$, equivalent to Eq. (14), is

$$\sum_{j=1}^{N_F} F_{nj} F_{mj}^* = \sum_{j=1}^{N_F} \frac{e^{i \operatorname{Re}[(k_n(f_j) - k_m(f_j))r_o]} }{N_F} \stackrel{?}{=} \delta_{nm}. \quad (23)$$

For this configuration n_{rot} , equivalent to Eq. (15), is given by

$$n_{\text{rot}} = \frac{r_o}{2\pi} \{ [k_n(f_{\text{max}}) - k_m(f_{\text{max}})] - [k_n(f_{\text{min}}) - k_m(f_{\text{min}})] \}, \quad (24)$$

where f_{min} and f_{max} are the minimum and maximum frequency of the band. As illustrated in Fig. 2, the matrix \mathbf{F} is approximately orthonormal when n_{rot} is large. To obtain the physical condition that corresponds to large values of n_{rot} , both sides of Eq. (24) are divided by the bandwidth B

$$\frac{n_{\text{rot}}}{B} = \frac{r_o}{2\pi} \left[\frac{k_n(f_{\text{max}}) - k_n(f_{\text{min}})}{B} - \frac{k_m(f_{\text{max}}) - k_m(f_{\text{min}})}{B} \right]. \quad (25)$$

For sufficiently small bandwidth, Eq. (25) reduces to

$$\frac{n_{\text{rot}}}{B} = r_o \left[\frac{1}{v_n} - \frac{1}{v_m} \right], \quad (26)$$

where $v_n = 2\pi df/dk_n$ is the modal group velocity. In terms of modal travel times, $\tau_n = r_o/v_n$, n_{rot} may be expressed as

$$n_{\text{rot}} = B(\tau_n - \tau_m). \quad (27)$$

Since a pulse of bandwidth B has a nominal duration of $1/B$, Eq. (27) implies that $n_{\text{rot}} > 1$ when the modal arrivals are temporally resolved.

2. Uncorrelated sources

In Ref. 3, it is stated that a sheet of uncorrelated, uniformly distributed sources near the ocean surface also produces a pressure matrix that can be expressed as a product of three matrices similar to Eq. (7). For this ambient noise case, the elements of the pressure matrix are the same as those in Eq. (2) except the range r_j corresponds to the range from the VLA to source j (see Chap. 9, Sec. 2.4 of Ref. 11). Arguments equivalent to those already presented lead to the conclusion that if the uncorrelated sources are distributed finely enough over a sufficiently large range interval, then the matrix analogous to \mathbf{R} in Eq. (10) satisfies $\mathbf{R}\mathbf{R}^\dagger \approx \mathbf{1}$, and the SVD of \mathbf{P} yields the depth-dependent modes.

There are inherent advantages and limitations to using either ambient noise sources or a traveling source of opportunity for the mode extraction. One apparent advantage of using ambient noise is that \mathbf{P} may be constructed using a relatively short time period, during which the sound-speed profile is likely to be constant. When using a traveling source, \mathbf{P} must be constructed using a time period that is

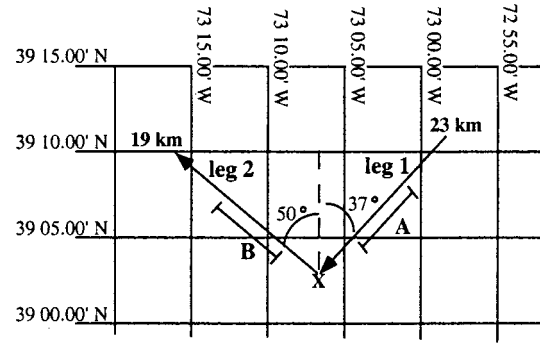


FIG. 3. Diagram of the first two legs of the ACT-II TL2 run. The X indicates the location of the VLA. The segments A and B indicate the range intervals used in Figs. 5–11.

sufficiently large for the source to traverse the required range extent, during which the sound-speed profile could fluctuate. On the other hand, a possible limiting factor in using ambient noise for the mode extraction is that the sources are likely to be distributed at all ranges. The presence of the short-range sources can lead to difficulty in the mode extraction, as described above, because the number of propagating modes may vary significantly. The shorter ranges can be more easily excluded when using a traveling source.

III. APPLICATION OF THE MODE EXTRACTION METHOD TO THE ACT-II DATA

The mode extraction method is now applied to experimental data. In this section, the Area Characterization Test II (ACT-II) and the data sets used for mode extraction are described. Examples of modes extracted from the data at the frequencies of a towed cw source while the ship traveled along (1) a constant-bathymetry (range-independent) track and (2) an up-slope (range-dependent) track are given. Results of mode extraction using ambient noise recorded on the VLA are also presented.

A. Source–receiver geometry

The ACT-II experiment was conducted in September 1993 in the Hudson Canyon area of the New Jersey Shelf. Mode extraction is performed using data obtained during run TL2 at a location called the AMCOR site, named after the nearby AMCOR 6010 borehole.^{12–14} An illustration of the first two legs of run TL2 is given in Fig. 3. Leg 1 lies along a region of basically constant bathymetry; leg 2 lies up-slope.

The VLA, indicated by the X in Fig. 3, consists of 20 vertical elements, 19 of which were connected to the SEACAL recording system. The interelement spacing and relative distance of each element from the ocean bottom are shown in Fig. 4. The water depth is approximately 73 m. The receivers are concentrated in the lower half of the water column, where the spacing is 1.905 m. The receiver spacing near the top of the water column is 7.62 m. The sparseness of the receivers in the upper part of the water column is not optimal for the mode extraction technique.

Data from the first two source tracks of run TL2 are used for mode extraction: (1) a range-independent leg (constant bathymetry) during which the ship traveled from a source–

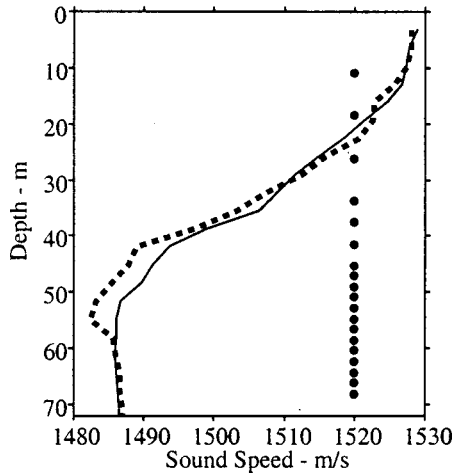


FIG. 4. The ACT-II VLA receivers (circles) and two of the sound-speed profiles obtained from XBTs. The solid line was measured at 0330 Z and the dashed line at 0212 Z, day 261.

VLA range of 22 km towards the array with a true bearing angle of 37 deg and a minimum source–VLA range of 1 km; and (2) a range-dependent leg (up-slope) during which the ship traveled out to a maximum source–VLA distance of 18 km with a true bearing of 310 deg. A J15-3 source projector emitted cw tones that were pulsed cyclically (see Ref. 7, Sec. 5.0) and was towed at a depth of 36 m.

B. The ocean environment

During the ACT-II experiment many sound-speed profiles were measured using conductivity–temperature–density casts (CTDs) and expendable bathy-thermograms (XBTs). Examples of the measured profiles are shown in Fig. 4; a more complete set may be found in Ref. 15.

Descriptions of the ocean bottom in the Hudson Canyon area are available from other experiments that have been performed in the area.¹⁶ A borehole known as AMCOR 6010 was drilled in 1976,¹² and seismic surveying was performed in the area.^{17,18} Geoacoustic profile values for the first 50 m of the ocean bottom from Ref. 15, with attenuation factors from Ref. 16, are listed in Table I.

C. Modes extracted from a range-independent track

Modes extracted using data from the middle of leg 1 of run TL2 are now presented. The results of mode extraction at 100, 150, and 200 Hz using data recorded from 0315 to 0420 Z, with $T_w = 0.63$ s, corresponding to approximate source–

TABLE I. Table of the sediment properties from Refs. 14, 15, and 17.

Depth (m)	c_p (m/s)	c_s (m/s)	ρ (g/cm ³)	α_p (dB/ λ)	α_s (dB/ λ)
5	1560	138	1.86	0.08	1.04
10	1610	182	1.96	0.13	0.82
20	1740	260	2.09	0.22	1.23
30	1830	326	2.17	0.18	0.82
40	1760	310	2.09	0.09	1.09
50	1710	299	2.03	0.16	1.06

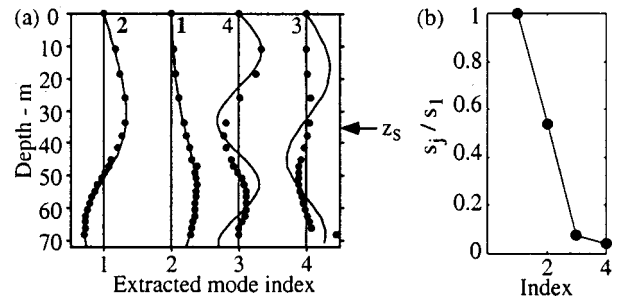


FIG. 5. (a) Extracted modes (dots) and predicted modes (lines) and (b) the corresponding scaled singular values obtained using the 100-Hz tone data recorded from 0315 to 0420 Z on day 261, leg 1 of run TL2, during which the ship traveled from ranges of approximately 14 to 6 km. The numbers at the top of part (a) are the modeled mode numbers.

VLA ranges of 14 to 6 km are shown in Figs. 5–7. This range interval is labeled section A in Fig. 3 and is sufficiently large to satisfy the range requirement as illustrated in Fig. 2. In part (a) of Figs. 5–7, the extracted modes at the VLA depths are indicated by the dots. The lines are the mode functions obtained from the ORCA normal mode model using measured sound-speed profiles, a nominal water depth of 73 m, and the historical bottom geoacoustic profile given in Ref. 17. The total number of modes shown in Figs. 5–7 equals the total number of modes found by the model at each frequency. The modes are generally well extracted. Discrepancies between extracted and modeled modes are expected and may be caused by either poor mode extraction or by inaccurate model inputs. The order of the extracted modes agrees well with the reported source depth of 36 m, since the mode function amplitudes at z_s decrease as the extracted mode index, which corresponds to the SVD column number, increases. For example, at 150 Hz in Fig. 6(a), a source depth closer to 50 m would lead to the extraction of modes 1 and 3 in the first two columns of \mathbf{U} instead of modes 2 and 4. Part (b) of Figs. 5–7 contains the scaled singular values. The singular values are shown to illustrate that extracted modes with close singular values can be degenerate even though many are well extracted. An example of degenerate modes is modes 3 and 4 at 100 Hz in Fig. 5(a). The corresponding difference in scaled singular values is 0.03 or 3% of the largest singular value.

The mode extraction technique works best at lower frequencies when the number of propagating modes is relatively small. However, to test the limits of the method and develop additional criteria, the results of mode extraction at 300, 400, and 500 Hz are shown in Figs. 8–10. To obtain the

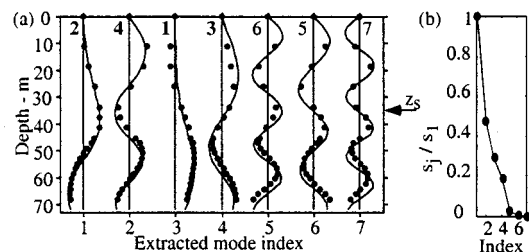


FIG. 6. Mode extraction results for the tone at 150 Hz. The format is the same as in Fig. 5.

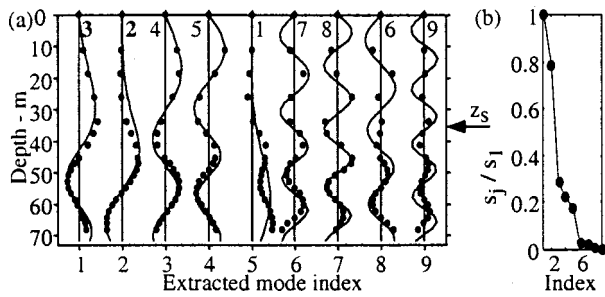


FIG. 7. Mode extraction results for the tone at 200 Hz. The format is the same as in Fig. 5.

best results at the higher frequencies, a larger coherent integration time, $T_w = 1.26$ s, is used to take advantage of the longer pulse duration and thus increase the SNR. Many of the low-order modes are well extracted, but, unfortunately, the high-order modes are not well sampled by the VLA in the upper part of the water column. The order of the well-extracted modes again agrees well with the source depth of 36 m. It is evident from part (b) of Figs. 8–10 that the probability that extracted modes are degenerate because of close singular values increases with frequency. If an approximate water depth is known, the degenerate modes can be identified as those that bear no resemblance to the modeled mode shapes (see, for example, extracted modes 7 and 8 at 400 Hz in Fig. 9).

In summary, mode extraction from a range-independent leg of the ACT-II experiment is quite successful and exhibits characteristics consistent with our theoretical development: the modes are extracted better at the lower frequencies; the higher-order modes cannot be well extracted unless they are well sampled in depth; and the source depth primarily determines the order of the extracted modes.

D. Modes extracted from a range-dependent track

Although the mode extraction technique was developed for a range-independent environment in Sec. II, we now show that the mode extraction also works for a mildly range-dependent environment. Using the adiabatic approximation, which assumes that the modes do not couple in a weakly range-dependent environment, the expression for the spectral components of the pressure field at a depth z and range r from a source as a sum over normal modes [see Eq. (2)] becomes

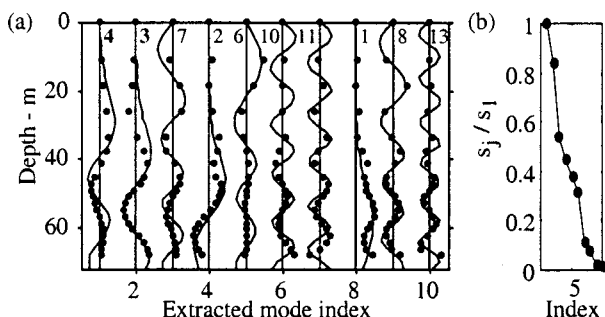


FIG. 8. Mode extraction results for the tone at 300 Hz. The format is the same as in Fig. 5.

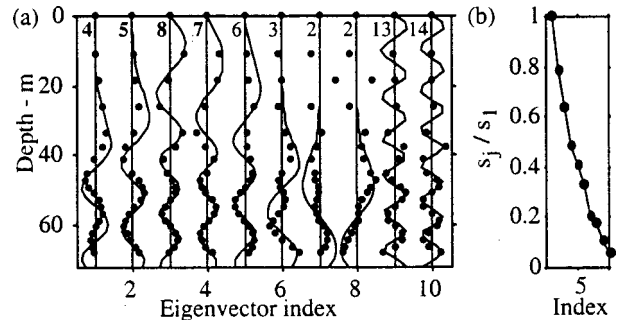


FIG. 9. Mode extraction results for the tone at 400 Hz. The format is the same as in Fig. 5.

$$p(z, r) = \frac{\sqrt{2\pi} e^{i\pi/4}}{\rho(z_s)} \sum_{n=1}^{\infty} \bar{\phi}_n(z_s, r_s) \bar{\phi}_n(z, r) \frac{e^{i \int_0^r k_n(r') dr'}}{\sqrt{\int_0^r k_n(r') dr'}}. \quad (28)$$

During leg 2 of run TL2, the ship traveled away from the VLA along an up-slope track. The change in water depth was approximately 12 m over 18 km. The results of mode extraction at the low frequencies using data taken from the middle of leg 2 are shown in Fig. 11. Specifically, data recorded from 0620 to 0740 Z, which correspond to approximate ranges of 6 to 15 km and are shown as section B in Fig. 3, are used. The modes are extracted well. Note that the order of the extracted modes in part (a) of Figs. 5–7 is different than the order in Fig. 11. In particular, mode 1, which has larger amplitude at lower depths, appears earlier in the columns of U at all three frequencies in Fig. 11, indicating a deeper effective source depth. The deeper effective source depth is reasonable because the mode shapes elongate as they travel down-slope from the ship to the VLA. In Ref. 19, a deeper effective source depth caused by adiabatic mode propagation is referred to as a “mirage.” Thus, the mode extraction technique does work for a range-dependent environment as long as the changes in range occur slowly enough or far enough from the VLA for the mode shapes to adapt to the environment at the VLA.

E. Modes extracted from ambient noise

Modes extracted using data recorded on the VLA from 0200 to 0210 Z, day 261 are now shown. During this time, the ship was at least 22 km from the VLA and the source for

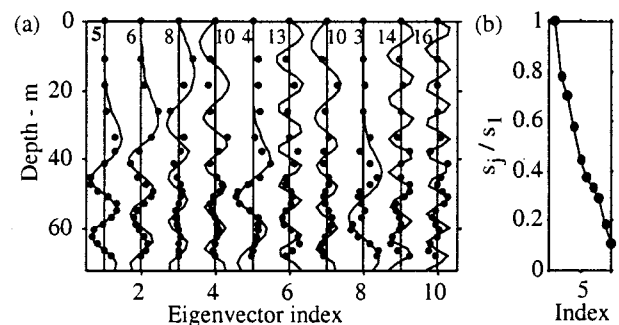


FIG. 10. Mode extraction results for the tone at 500 Hz. The format is the same as in Fig. 5.

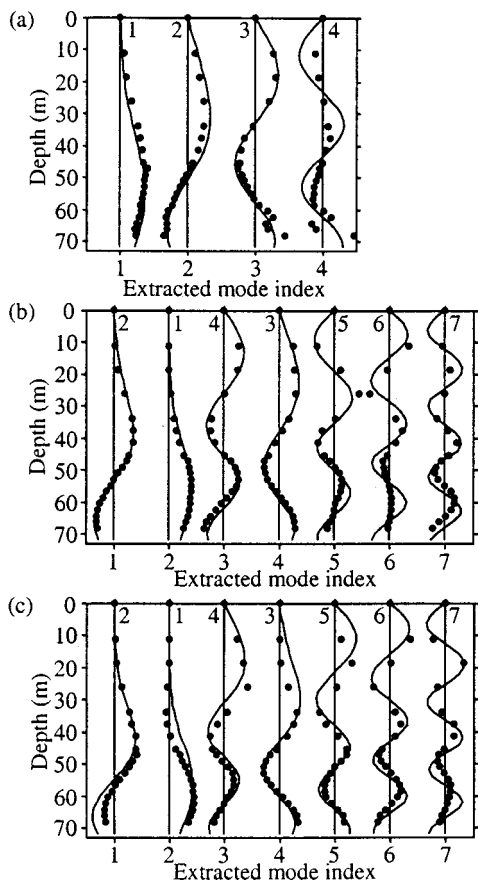


FIG. 11. Modes extracted at 100 Hz (a); 150 Hz (b); and 200 Hz (c) from data recorded from 0620 to 0740 Z on day 261 during range-dependent leg 2 of run TL2. The approximate range interval is 6 to 15 km.

the cw tones was not yet on. The signal processing is performed using a coherent integration time of $T_w = 0.16$ s and a 50% overlap. The frequency bin size corresponding to this integration time is 6.4 Hz; thus, the data are averaged over a 6.4-Hz frequency band during the Fourier transform. This resulted in 7420 time samples over the 10-min time interval that was used to form the cross-spectral density matrix.

Figure 12 shows the first five modes extracted from the resulting cross-spectral density matrix at (a) 120 Hz; (b) 250 Hz; and (c) 350 Hz. Many of the extracted modes have excellent correlation with the modes modeled using the sound-speed profile from an XBT measurement taken at 0212 Z.

The order of the extracted modes gives an approximate value for the effective source depth of the ambient noise. The primary extracted modes all have larger amplitudes at depths of less than 10 m than the modes that appear in subsequent columns of U . Thus, the effective source depth for the ambient noise implied from the mode extraction is less than 10 m. A shallow source depth for the ambient noise is logical because the sound recorded during the time interval 0200 to 0210 Z was most likely associated with surface noise.

IV. SUMMARY

In this paper we have presented an approach for extracting mode functions from data measured on a vertical line array and applied the method successfully to experimental data. The mode extraction technique is predicted to work

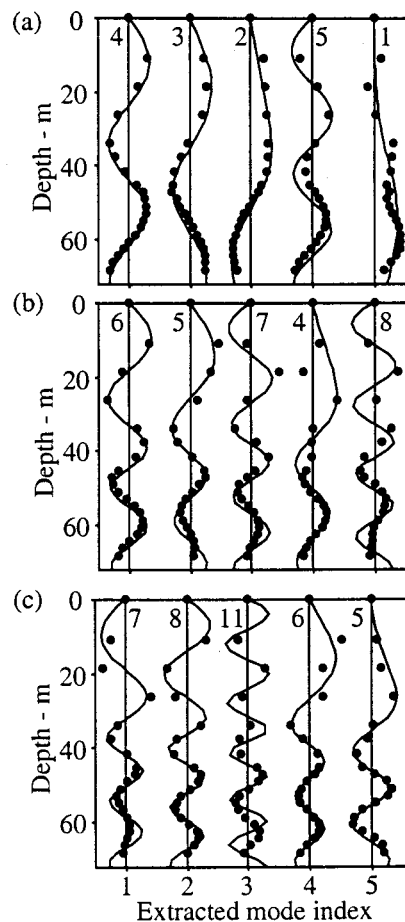


FIG. 12. Modes extracted from ambient noise recorded prior to the experiment at (a) 120 Hz; (b) 250 Hz; and (c) 350 Hz.

well if the VLA samples the water column well and if either a single source covers a sufficient range extent or a large number of uncorrelated sources produce the field, as in the case of ambient noise from the ocean surface. In the single-source case, the acoustic source need not be controlled: its depth, the phase of its tonals, and its precise track do not need to be known. Also, the ocean environment need not be known.

The mode extraction technique was applied to the ACT-II data set. Despite the relative sparseness of the array near the top of the water column, depth-dependent normal modes were successfully extracted using data acquired in both range-independent and slightly range-dependent environments. Modes were also successfully extracted from ambient noise.

Depth-dependent modes obtained using this mode extraction technique may be used as inputs for additional data analysis. For example, in Ref. 20, the data-extracted modes may be used in environmental inversions to obtain properties of the upper sediment layer. In Ref. 6, depth-dependent mode functions and horizontal wave numbers are calculated using a VLA that partially spans the water column, and the resulting data-derived modes and wave numbers are used in matched-field processing.

ACKNOWLEDGMENTS

This research was sponsored by the Office of Naval Research. We thank the authors of Refs. 4 and 6 for providing preprints of their work, and the reviewers for their helpful comments.

- ¹C. T. Tindle, K. M. Guthrie, G. E. J. Bold, M. D. Johns, D. Jones, K. O. Dixon, and T. G. Birdsall, "Measurements of the frequency dependence of normal modes," *J. Acoust. Soc. Am.* **64**, 1178–1185 (1978).
- ²S. N. Wolf, D. K. Cooper, and B. J. Orchard, "Environmentally adaptive signal processing in shallow water," in *Oceans '93, Engineering in Harmony with Ocean Proceedings* (IEEE, Piscataway, NJ, 1993), Vol. 1 of 3.
- ³P. Hursky, W. S. Hodgkiss, and W. A. Kuperman, "Extracting modal structure from vertical array ambient noise data in shallow water," *J. Acoust. Soc. Am.* **98**, 2971 (1995).
- ⁴G. B. Smith, "'Through the sensor' environmental estimation," *J. Acoust. Soc. Am.* **101**, 3046 (1997).
- ⁵T. B. Neilsen, and E. K. Westwood, "Mode function extraction from a VLA using singular value decomposition," *J. Acoust. Soc. Am.* **101**, 3025 (1997).
- ⁶P. Hursky, W. S. Hodgkiss, and W. A. Kuperman, "Matched field processing with data-derived modes," *J. Acoust. Soc. Am.* **109**, 1355–1366 (2000).
- ⁷J. Kwon, O. Marcia, and C. Brundick, "ACT-II reconstruction data base," BBN Systems and Technologies, Arlington, VA, BBN Tech. Memo W1208, May 1994.
- ⁸E. K. Westwood, C. T. Tindle, and N. R. Chapman, "A normal mode model for acousto-elastic environments," *J. Acoust. Soc. Am.* **100**, 3631–3645 (1996). The general orthonormality condition satisfied by the mode functions is given in Eq. (12) therein.
- ⁹W. H. Press, A. Teukolsky, W. T. Vetterling, and B. P. Flannery, *Numerical Recipes in FORTRAN: The Art of Scientific Computing* (Cambridge University Press, Cambridge, 1992).
- ¹⁰Although Ref. 9 states that the singular vectors are degenerate when the singular values are *exactly* equal, we have found, using simulated data with ideal range and depth sampling, that the singular values only need to be *relatively* close to one another for the extracted modes to be invalid.
- ¹¹F. B. Jensen, W. A. Kuperman, M. B. Porter, and H. Schmidt, *Computational Ocean Acoustics* (AIP, New York, 1994).
- ¹²J. C. Hathaway, C. W. Poag, P. C. Valentine, R. E. Miller, D. M. Schultz, F. T. Manhiem, F. A. Kohout, M. H. Bothner, and D. A. Sangrey, "U.S. geological core drilling on the Atlantic shelf," *Science* **94**, 515–527 (1976).
- ¹³T. Yamamoto, M. V. Trevorrow, M. Badiy, and A. Turgut, "Seabed porosity and shear modulus inversion using surface gravity (wave) water-induced seabed motion," *Geophys. J. Int.* **98**(1), 173–178 (1989).
- ¹⁴M. V. Trevorrow and T. Yamamoto, "Summary of marine sedimentary shear modulus and acoustic speed profile results using a gravity wave inversion technique," *J. Acoust. Soc. Am.* **90**, 441–455 (1991).
- ¹⁵D. P. Knobles, E. K. Westwood, and J. E. LeMond, "Modal time-series structure in a shallow-water environment," *IEEE J. Ocean. Eng.* **23**, 188–202 (1998).
- ¹⁶W. M. Carey, J. D. Douth, R. B. Evans, and L. M. Dillman, "Shallow-water sound transmission measurements on the New Jersey continental shelf," *IEEE J. Ocean. Eng.* **20**, 321–336 (1995).
- ¹⁷T. A. Davies, J. A. Austin, M. B. Lagoe, and J. D. Milliman, "Late quaternary sedimentation off New Jersey: New results using 3D seismic profiles and cores," *Mar. Geol.* **108**, 323–343 (1992).
- ¹⁸R. D. Stoll, G. M. Bryan, R. Mithal, and R. Flood, "Field experiments to study seafloor seismoacoustic response," *J. Acoust. Soc. Am.* **89**, 2232–2240 (1991).
- ¹⁹G. L. D'Spain, J. J. Murray, W. S. Hodgkiss, N. O. Booth, and P. W. Schey, "Mirages in shallow-water matched-field processing," *J. Acoust. Soc. Am.* **105**, 3245–3265 (1999).
- ²⁰T. B. Neilsen and E. K. Westwood (unpublished).